Journal of New Technology and Materials
JNTM
Vol. 01, N°00 (2011)8-23

OEB Univ. Publish. Co.

Nanopowders prepared by Solar Physical Vapor Deposition (SPVD)

Claude J. A. Monty
CNRS, PROMES laboratory, Odeillo, Font-Romeu, 66120 France
claude.monty@promes.cnrs.fr
Received: 23 May 2011, accepted as plenary talk

Abstract
The Solar Physical Vapor Deposition (SPVD) is an original process to prepare nanopowders. This method has been developed in Odeillo-Font Romeu in France using solar reactors working under concentrated sunlight in 2kW solar furnaces. Various oxides, pure or containing other elements in addition, have been obtained. This paper focus on ZnO and TiO_2. based oxides It is shown that the X-Rays Diffraction analysis allows a fine nanostructural characterisation of the nanophases present in these nanopowders. In many cases, HRTEM or SEM and XPS complement the XRD analysis. The properties such as Electrical, magnetic properties, photoreactivity, luminescence ... known on microstructured materials of the same composition are revisited on these nanopowders or on nanomaterials prepared from them and led in many cases to original behaviours.
Keywords : SPVD, nanopowders, Al doped ZnO, Co doped ZnO, Bi_2O_3, TiO_2, XRD, HRTEM, chemical reactivity, magnetic properties, electrical conductivity.

1. Introduction

An original process to prepare nanopowders : the Solar Physical Vapor Deposition (SPVD) is presented[1]. Pure ZnO, $Zn_{1-x}Al_xO$, $Zn_{1-x}Co_xO$, $Zn_{1-x}Bi_xO$ and metallic Zn nanophases as well as pure TiO_2 and Fe, Co or Mn-doped TiO_2 have been prepared by this method which we have initially used to prepare simple nanophases of good quality : $Zr_{1-x}Y_xO_2$, γ-Fe_2O_3, In_2O_3, SnO_2... [2-5].

In some experiments, nanopowders appeared to be a mixtures of nanophases, it was the case of $(Zn_{1-x}Bi_xO)$ and $(Bi_{1-y}Zn_y)_2O_3$.obtained both in unequal quantities, but also the case of metallic Zn obtained beside strongly reduced ZnO_{1-x}. and of TiO_2 nanopowders which are generally a mixture of rutile and anatase. Composite nanoparticles such as MgO coated Fe nanoparticles can be also prepared by SPVD.

To characterize the nanostructure and the composition of the nanopowders the main method used was X Ray Diffraction (XRD) analysis. The nanostructure and detailed information on the nanophases present in the nanopowders are studied too by High Resolution Transmission Electron Microscopy (HRTEM) or by Scanning Electron Microscopy (SEM). Energy Dispersive X-ray analysis (EDX) and X-ray Photoelectron Spectroscopy (XPS) bring in some cases complementary information on the chemical state of the nanopowders. Studies have been performed to know more about their chemical reactivity, their magnetic or/and their luminescence properties. In the case of nanopowders prepared by SPVD from targets made by sintering ZnO and Bi_2O_3, nanostructured ceramics could be obtained and their electrical properties studied

The properties found are clearly related to the composition and the nanostructure of the nanopowders prepared by the SPVD process. Most of studies were performed in collaboration and important papers are cited in references but in this paper, some striking results obtained on ZnO and TiO_2 based nanomaterials have been revisited.

2. Nanopowders and massive nanomaterials

Nanopowders are formed of grains (unorganised aggregates, nanocrystals or polycrystals) which have nanometric dimensions ; they belong to the general class of "nanomaterials". It is known that nanomaterials properties are strongly influenced by the interfaces present (surfaces, grain boundaries...)[3, 2].

Dimensional and microstructural criterions can be used to classify a material among the nanomaterials ones[2, 6]. These criterions have the merit to recall that well before the appearance of nanomaterials, the solid state physicists were interested in aggregates of some atoms and the effects of their size on the electronic and crystallographic structures [7]. In the same way, the chemists knew for a long time that the chemical reactivity of small particles is much higher than that of ordinary powders this property is used in catalysis.

It is not surprising when a property is studied as a function of the grain size (or the thickness of a layer deposited on a substrate), to observe an "abnormal" behavior for grains sizes or a thickness smaller than around 100 nm. The "critical size" depends on the sensitivity of the properties studied on the interfaces and their thermodynamic state. For the same material it varies with the property and with the thermo-mechanical history of the material.

Technologies are in progress from about 20 years now to prepare films or coatings and massive nanomaterials directly or from the nanopowders obtained by various methods. In the following an original process to prepare nanopowders is described: the Solar Physical Vapor Deposition (SPVD) and some typical results obtained on selected oxides are gathered and compared [4-5, 8-10, 6, 11-12].

3. The Physical Vapor Deposition process in a Solar reactor (SPVD)

3-a The solar reactor « Heliotron »

A 1MW solar furnace was built in Odeillo/Font Romeu around 1970. In the same building and beside, ten 2kW solar furnaces and a 10 kW more easy to handle can be used for laboratory experiments at a smaller scale. They are constituted by mobile plane mirrors ("heliostats") tracking the sun and reflecting the radiation on a parabolic concentrator. At the focus where the concentration can be as high as 18000 on a surface of around 10 mm^2, are placed more or less sophisticated reactors or experimental set ups.

For the SPVD experiments, the reactors are constituted by glass balloons (see figure 1). Inside, a target, made with the material to be melted and vaporized or sublimated (depending on its nature), is placed on a cooled support at the focus of the concentrator. The vapor pressure around the target depends on the material and on the atmosphere inside the balloon, it is more or less large. In the last case, a smoke is generally visible and is depositing by condensation on a cold finger (water cooled copper tube)[4]. In a similar reactor, the smoke is collected on a metallic or a nanoporous ceramic filter through which the gas atmosphere is flowing.

The "heliotron", associates the two processes (see figure 1) : collection by trapping on a cold finger and pumping through a filter, which decreases the phenomena of condensation on the walls of the balloon and increases the effectiveness of the collection. The production rate of the nanopowders depends on the vapor pressure of the material. In the best cases (for example pure or doped zinc oxide), it can reach several hundred milligrams per hour.

When the vapor pressure on the top of the melted material is low, which is the case of alumina or doped zirconia for examples, it is less than 1 mg/hour in a sunny period (flux higher than $1kW/m^2$). It is one of the reasons why in that case, when large quantities are needed, a different process has been developed, associating melting in a solar furnace, quenching and ball milling[6].

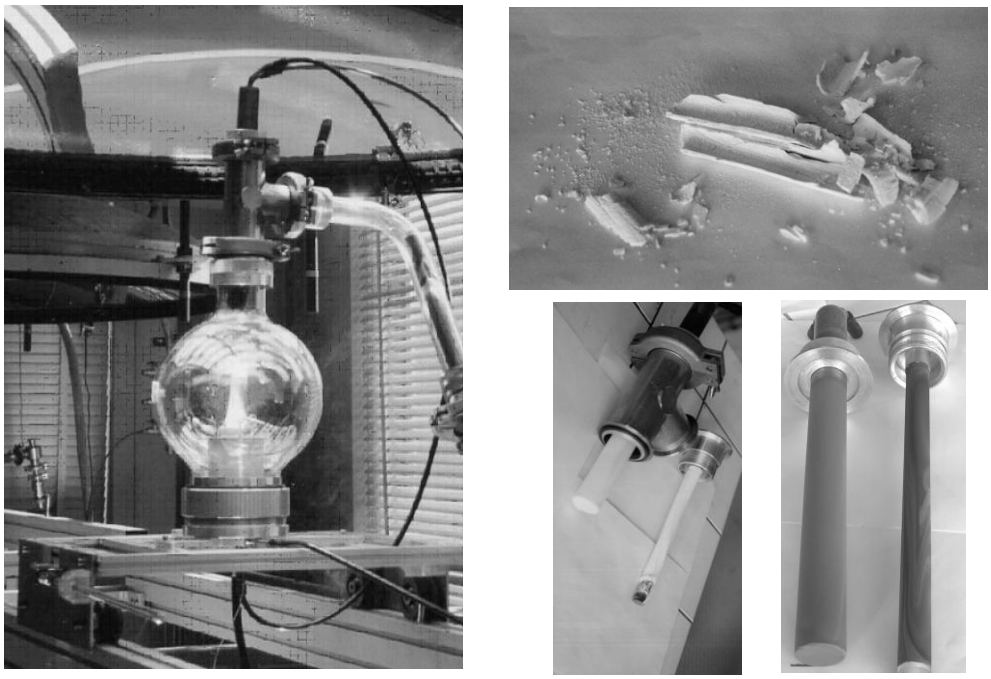

Figure 1 – SPVD process in the Heliotron solar reactor. Nanopowders are collected simultaneously on a ceramic (or metallic) filter and on a water cooled copper finger. In the case of ZnO, the nanophases are white fibers. Under Ar flow the collected grey nanopowders are a mixture of Zn and highly reduced ZnO.

3-b Nanophases prepared by SPVD or SCVD

Using "heliotron" type solar reactors in 2kW furnaces SPVD appeared to be an excellent process to prepare nanophases. Depending on the composition of the targets, the oxide nanopowders obtained were formed by one type of nanophases : ZrO_{2-x}, SnO_{2-x}, MgO, In_2O_3, CeO_2, gadolinium doped ceria $Ce_{1-x}Gd_xO_{2-\delta}$, yttrium doped zirconia $Zr_{1-x}Y_xO_{2-\delta}$, TiO_2 (Anatase or Rutile) and pure or doped zinc oxide nanophases : ZnO, $Zn_{1-x}In_xO$, $Zn_{1-x}Sb_xO$, $Zn_{1-x}Al_xO$, $Zn_{1-x}Co_xO$, $Zn_{1-x}Bi_xO$, β-$Bi_2O_{3-\delta}$. [4-5, 8-10, 6, 12]. Starting from targets made by sintering ZnO and Bi_2O_3, mixtures of $(Zn_{1-x}Bi_xO)$ and $(Bi_{1-y}Zn_y)_2O_{3-z}$. nanophases were prepared[11]. More recently composite nanoparticles such as MgO coated Fe could also be prepared, playing on the target composition and the oxydo-reduction properties of the atmosphere[13]. In reducing atmospheres (Ar or N_2) ZnO leads at high temperature to metallic Zn particles mixed with a small proportion of ZnO nanophases[12]. SPVD of AlN in hydrogenated argon lead to metallic Al nanophases (in such a case Solar Chemical Vapor Deposition or SCVD is a more adequate terminology than

SPVD. Nanophases of Si and SiO_x were produced starting from silicon targets in a reactor whose vacuum was improved[14]. Large quantities of fullerenes and nanotubes were prepared by the same method in the 1 MW solar furnace of Odeillo by using a special 50 kW reactor with a graphite chamber[15].

In many cases, chemical reactions occur during the process and Solar Chemical Vapor Deposition, or SCVD, is a more adequate terminology than SPVD.

In the following some examples taken in the previous ones are considered.

4. Characterization of the nanopowders by X-Ray Diffraction

The first method used to characterize the powders after synthesis is the X-ray diffraction analysis (XRD). In the case of nanopowders, the diffraction peaks are widened compared to diffraction peaks obtained on micrometric powders. The Scherrer relation[16-17] can be used to determine the average size of the "fields of coherence" of diffracting domains of the analyzed powder and to compare it to the average grain size determined by other methods (HRTEM for example). Observations by scanning electron microscopy (SEM) or by transmission electron microscopy (TEM and HRTEM) are useful methods to achieve the nanostructural studies made by XRD. XPS analysis gives access to the nanochemistry of the nanophases, constituting the nanopowders.

4-a X-rays diffraction diagram

The X-ray diffraction peaks obtained from a crystallized powder are characterized by diffraction angles θ_{hkl} and I_{hkl} intensities depending on the lattice cell and on the λ wavelength radiation, used. The hkl Miller indexes correspond to the diffracting crystallographic planes (d_{hkl} is the distance between them). These three parameters are connected through the Bragg relation :

$$2d_{hkl} \sin \theta_{hkl} = n\lambda \qquad (1)$$

The position of the diffraction peaks gives access to the distances d_{hkl} between crystallographic planes, the structure and the lattice parameters.

If a monochromator is used, λ is perfectly defined. In order not to loose intensity, two close wavelengths are used simultaneously; it is the case with a copper anti-cathode whose the emission spectra contains the two close wavelengths $\lambda_{K\alpha1}$= 1.540562 Å and $\lambda_{K\alpha2}$= 1.54390 Å.

A fit of each diffraction peak by two Lorentz functions, corresponding to $\lambda_{K\alpha1}$ and $\lambda_{K\alpha2}$ wavelength, can be carried out by using for example the ORIGIN software. These functions have the following form :

$$y = y_0 + \frac{2A}{\pi} \frac{w}{4(x-x_0)^2 + w^2} \qquad (2)$$

in which :

y_0 is the value of the continuous background taken at the origin ;

A is the total area under the curve after subtraction of the background ;

x_0 is the x-coordinate to the maximum of the y-coordinate ;

w is called the Full Width of the peak at Half Maximum y value (FWHM).

These functions fit to the profiles of diffraction peak and specially allow a very good evaluation of FWHM. The peak area (parameter A) obtained using these functions is however known with some error. To calculate "the integral width", $A/y(x_0)$, it is for example, more accurate to fit the peak profiles with pseudo-Voigt functions. The diffraction peak width has to be corrected by an "instrumental width" w_{st}. The shape and the intrinsic width w_{in} of the diffraction peaks are dependent on the dimensions of the coherence diffraction domains called the "grain size" and on their mechanical state (strains). In classical materials without stresses and well crystallised over a micron scale, the peak width w and the instrumental width w_{st} are equal (w_{in} is nul or very small), but in nanomaterials they differ significantly. Langford et al. (1986)[17] have proposed a method to separate both effects plotting $w_{in} \cos\theta$ as a function of $\sin\theta$ leads for the same crystallographic plane family to a line with a positive slope or to a constant line, depending on the fact there are strains or not in the material. This method provides too a good determination of the peak's position x_0, associated to a given wavelength, which can be used to determine accurate values of the lattice parameters.

The intensity of the diffraction peaks (maximum of y in the relation 2) is connected to the crystallographic structure by the "structure factor" which takes into account the arrangement of the atoms and the distribution of grain orientations (texture). If the peak width are different from the instrumental peak width, the texture effects can be determined considering the integrated intensities (parameter A of the fitting function).

4-b Determination of the grain size

From the fits obtained on the experimental peaks, it is possible to determine the "intrinsic width" w_{in} of the diffraction peaks and to compute an "average grain size" d_m, using the relation (3) proposed by Scherrer :

$$d_m = K\lambda / w_{in} \cos\theta \qquad (3)$$

where

- d_m is the average size of crystallites
- K is a constant which depends on the form of the crystallites and on the Miller indexes [16] showed that in main cases the value of K is close to 0.9) ;
- θ is the Bragg diffraction angle ;
- λ is the wavelength of the incidental radiation ;
- w_{in} is the intrinsic width of the diffraction peak (measured in radians) which can be determined from the relation : $w^2_{in} = w^2 - w^2_{st}$ (strictly valid for Gaussian peak profiles).
- w corresponds to FWHM (see earlier).
- w_{st} is the instrumental width, i.e. the value of w obtained on reference crystals.

The use of this formula imposes to know the "instrumental function". That has been done using pure ZnO or LaB_6 polycrystals as reference materials.

4-c Instrumental function

To determine the "instrumental function", it is necessary to perform XRD on a reference material with large grain sizes and without strains. A pure ZnO powder has been annealed in air at 1400°C during 48h in such a way to obtain a large grain size. The X-Ray Diffraction diagram obtained is shown in the figure 2.

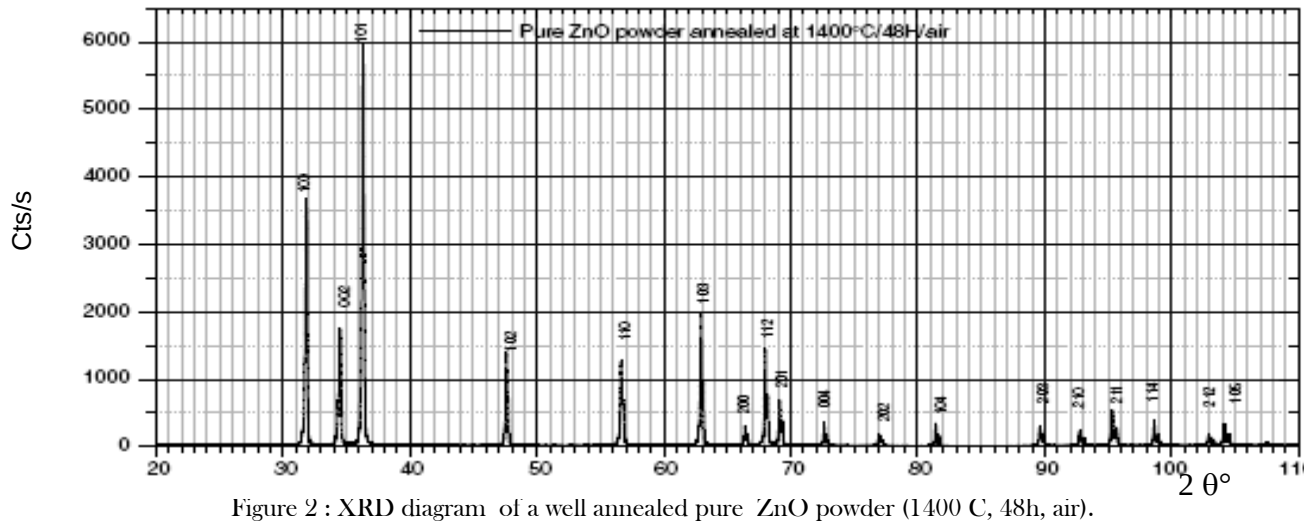

Figure 2 : XRD diagram of a well annealed pure ZnO powder (1400 C, 48h, air).

The intensities of the diffraction peaks of the diagram shown in figure 2 correspond to the XRD diagrams of the ICDD reference file (36-1451) and to the zincite hexagonal structure from the American Mineralogist Crystal Structure Database. Using these data of the atomic positions in the computer software CaRIne[18] leads to a quite similar diagram.

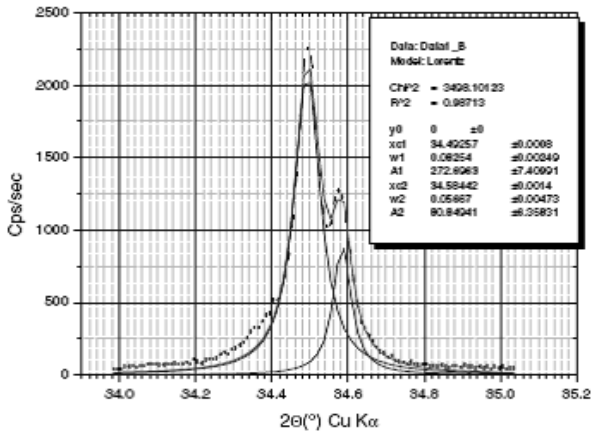

Figure 3 Decomposition in two Lorentz functions of the 002 peak of the XRD diagram seen in figure 2.

XRD spectra were analysed according to the criteria defined previously. Figure 3 shows an example of decomposition of the 002 peak in two Lorentz functions corresponding to the two components $\lambda_{K\alpha1}$ and $\lambda_{K\alpha2}$ of the wavelength $\lambda_{K\alpha}$ of copper. This procedure leads to define the "instrumental width" for each peak ; it has been applied to the whole diagram. The instrumental function can be defined as a fit to these experimental points ; the results obtained in this study are reported in the figure 4 beside similar results obtained using a LaB_6 polycrystal. Note the dispersion of the experimental points obtained on ZnO related to specific crystallographic directions, they are very close of those obtained by Langford et al. (1986)[17] : despite the fact that the instrumental function obtained correspond to the smallest FWHM values (obtained among several experiments), it is influenced by the microstructure. LaB_6 is then the best reference which can be used to characterize all the nanomaterials studied (as far as the XRD experimental set up is not modified). Nevertheless, the influence due to the difference between these two references is important only when the particles have large sizes i.e. higher than 100 nm.

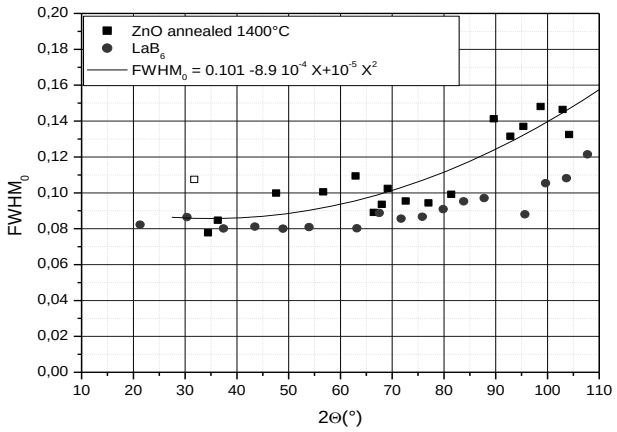

Figure 4 : Instrumental function determined using a LaB_6 polycrystal and compared to the values obtained from the diagram of figure 2.

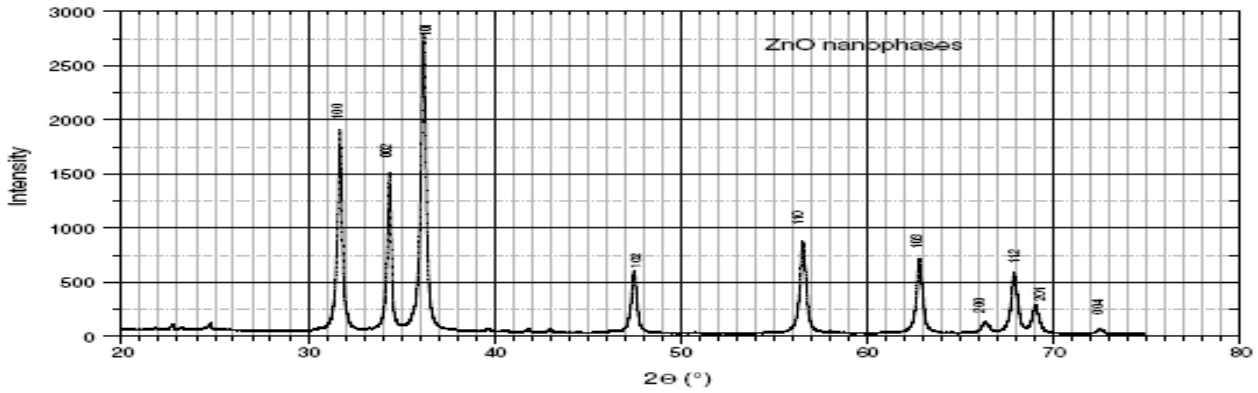

Figure 5 : XRD diagram of a ZnO nanopowder obtained by SPVD.

5. Characterisation and properties of ZnO based nanopowders prepared by SPVD

5-a SPVD nanopowders of pure ZnO

ZnO is a good example of oxide which can be prepared effectively in the form of nanophases by SPVD. The XRD diagram obtained on nanopowders (see figure 5) can be compared to the diagram obtained on annealed pure ZnO powder (fig 2).

Several observations can be made :

- The positions of the diffraction peaks of the nanopowders are, at first approximation, the same as those of a theoretical diagram computed taking an hexagonal cell with a = 3.24 Å and c = 5.20 Å.
- The diffraction peaks of the nanopowders are widened compared to those which are observed on a ZnO annealed powder, that is evident on the decomposition of 002 peak in figure 6 compared to the figure 3.

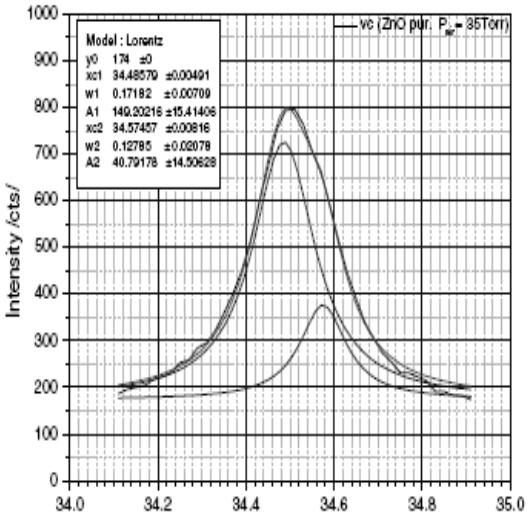

Figure 6 : Decomposition of the 002 peak of the XRD diagram of the figure 5.

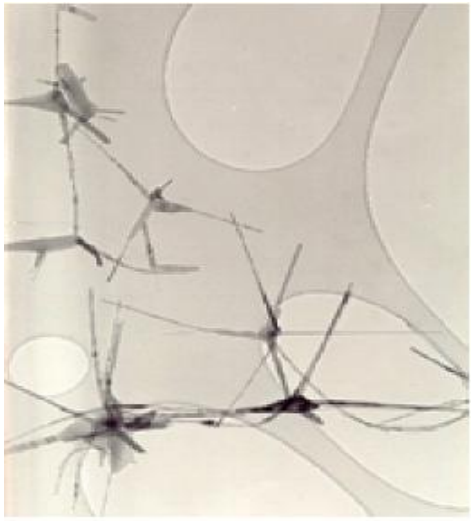

Figure 7 : TEM image of ZnO nanophases prepared by SPVD (x50000)

XRD changes indicate important size effects. The observation by TEM of SPVD powders obtained under 70-100 Torr of oxygen pressure, has shown elongated particles like rods, tetraedraly arranged 4 by 4 (see figure 7)[8].

When the morphology of the nanophases is anisotropic, it is possible by XRD to determine their average form from the "average sizes" of the particles along the principal crystallographic directions. It is however necessary to take into account that it is the average size of the coherence diffraction domains which are related to the size and morphology of the substructure. The determination of the size distributions and the morphology of the particles can be refined by observations in electron microscopy (HRTEM or SEM). This phenomenon appears too in the work performed by Langford et al. (1986)[17] and is generally observed in all the experimental XRD spectrum determined on ZnO.

5-b Grain size determination of pure ZnO nanopowders

Relation (3) has been used to calculate the coherence diffraction domain size d_m ("grain size") for the peaks obtained on ZnO SPVD nanopowders. The values obtained have been reported in figure 8 as a function of 2θ and of the origin of the starting powder: hydrothermal[19-20] or plasma synthesis[21]. The method applied to a broad field of the XRD diagrams permitted in the case of ZnO to highlight the shape anisotropy of the coherence diffraction domains. It can be seen indeed that the dimensions obtained depend on the crystallographic directions considered. The peaks corresponding to the crystallographic directions [00l] (reflecting planes parallel to the basic plane and perpendicular to the c axis) have a smaller width than that of the hk0 peaks (reflecting planes containing the c axis). The average shape of the coherence diffraction domains can thus be represented by an ellipsoid lengthened along the c axis. That is confirmed by HRTEM observations showing that under air pressures of 70-100 Torr, the nanophases are whiskers (see figure 7). Nevertheless when the starting powder has been prepared by a plasma process the [200] direction corresponds also to large sizes. That could be interpreted like due to a preferential lengthening in a direction perpendicular to the c axis for a part of the nanoparticles. However, the accuracy of these determinations to the large diffraction angles remains smaller than with the small angles (more raised intensities, less recovering between peaks...). The fact that [100] direction does not indicate the same phenomenon, do not permit to interpret these observations in spite of their systematic character.

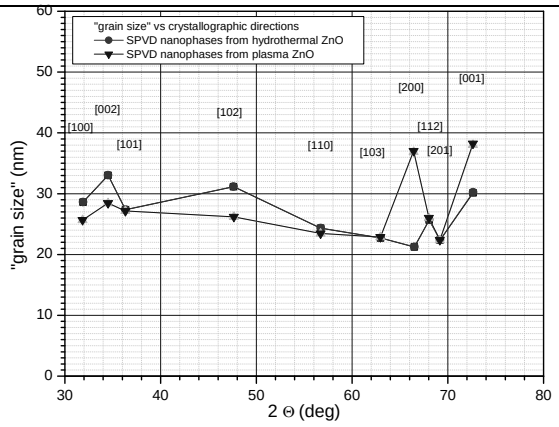

Figure 8-a : Coherency domain size ("grain size") as a function of crystallographic directions in ZnO nanopowders prepared by SPVD.

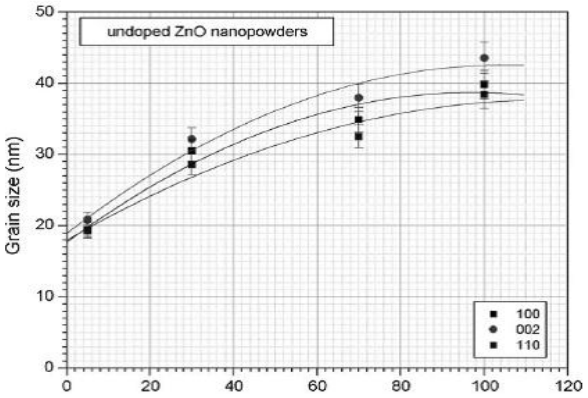

Figure 8-b : Influence of the air pressure on the grain size and shape anisotropy during the SPVD process.

A study of the influence of the air pressure inside the solar reactor on the grain size during the SPVD process has shown that increasing the pressure, increases the grain size along the c-axes and in perpendicular directions as well (see figure 8-b)[11].

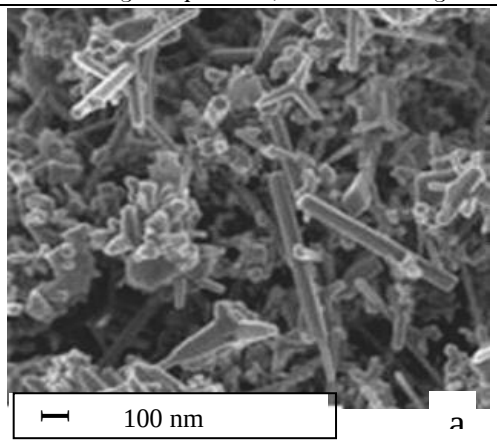

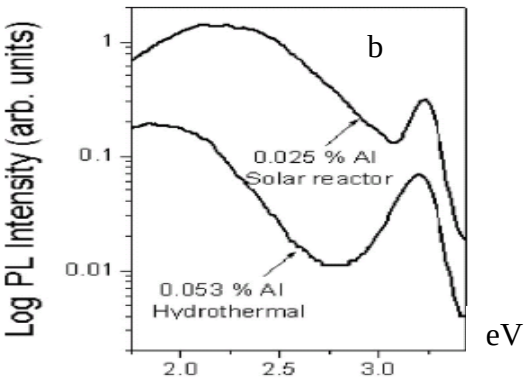

Figures 9-a -SEM image of a 0.16wt% Al doped ZnO nanopowder prepared by SPVD.
Figure 9-b –Photoluminescence of Al-doped nanopowders :
comparison of SPVD nanopowders with hydrothermal nanopowders.

5-c Al-doped ZnO nanopowders

Al doped ZnO nanopowders have been obtained by SPVD starting from powders prepared by an hydrothermal method[20] and containing 0.045wt% Al. The final content after vaporisation-condensation was 0.016wt%[23]. The image in figure 9-a shows an aspect of these nanopowders.

The nanopowders exhibit a photoluminescence in the blue range. It is clear that SPVD nanopowders have an intensity which is about an order of magnitude higher than the hydrothermal nanopowders from which they are issued, but they have lost a part of the doping element during the SPVD process.

SPVD nanopowders of Al doped ZnO obtained by a plasma process have been prepared[22]. The plasma method leads to introduce larger quantities of aluminium than the others methods. The nanopowders have been characterized by XRD in a similar way as it has been done for pure ZnO nanophases,. Figure 10-a shows the variations of average dimensions of the coherence diffraction domains determined as a function of the Al content of the powders.

These "grain sizes" vary with the direction in a similar way to those of the nanopowders of pure ZnO discussed previously. It was found nevertheless that the grain size increases when the Al content increases and, in the same time, the anisotropic shapes of the coherence diffraction domains are changing from a mixture of rods elongated along [001] and platelets perpendicular to [001], to mainly long rods.

The luminescence properties of Al doped ZnO nanopowders obtained by SPVD from targets prepared by a plasma process has been studied by Grigorjeva et al.[22]. An important result is a pure and intense blue light emission at 3.27 eV clearly related to the Al content of the doped ZnO nanopowders and to the SPVD process[22] (see figure 10-b).

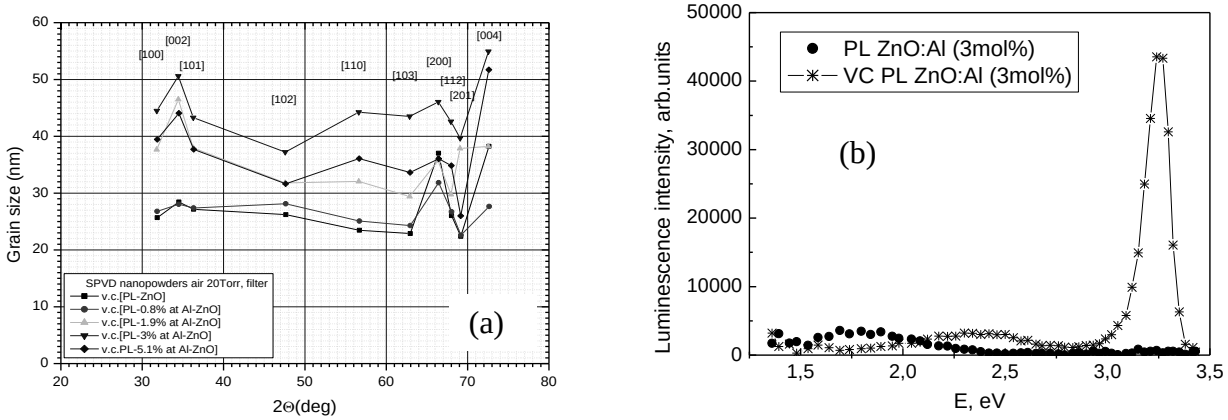

Figure 10-a: "grain size" as a function of the crystallographic direction for nanophases prepared by SPVD from Al doped ZnO obtained by a plasma process.

Figure 10-b : Blue emission of SPVD nanophases obtained by SPVD (noted VC) from Al doped ZnO (3%mol) targets prepared by a plasma process[22].

5-d Co-doped ZnO nanopowders

Co doped ZnO nanopowders were prepared by SPVD in order to study their magnetic properties. The anisotropic shape of the coherence diffraction domain observed in the case of pure ZnO is also highlighted in ZnO doped Co. The average "grain size" is around 20 nm and does not depends on the Co content. This has been also observed by transmission electron microscopy (see figures 11).The morphology of the nanopowders of Co doped ZnO is sensitive to the pressure maintained in the reactor during the SPVD process.

The magnetic properties of Co doped ZnO SPVD nanopowders were studied. For 5% at. Co doped ZnO prepared by SPVD under low air pressure, a ferromagnetic state appears with an hysteresis cycle and low coercitive field (approximately 100 Oe) at 5K and a saturation magnetisation. However these powders are superparamagnetic at the ambient temperature when they are prepared under air pressures of about 70-100 Torr [24].

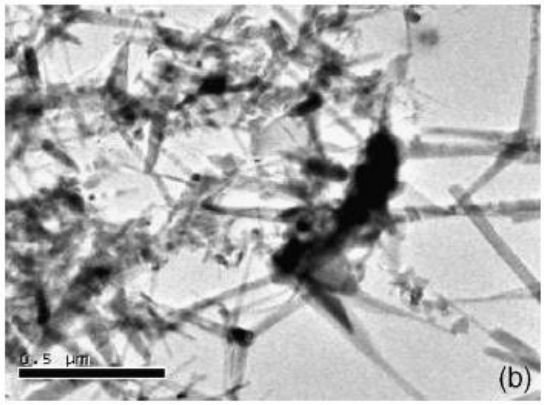

Figure 11 : Transmission Electron Microscopy of Co doped ZnO nanophases prepared by SPVD under 70-100 Torr air pressure.

5-e (ZnO)$_x$(Bi$_2$O$_3$)$_y$ nanopowders

Targets made of mixtures of ZnO and Bi_2O_3 with three compositions (5, 12 and 20 wt. %Bi_2O_3) were prepared and annealed under air at 700°C during 8 h to 17 h. The XRD analysis of these targets shows that two phases are present : $Zn_{1-x}Bi_xO$ and $Bi_{38}ZnO_{58+\delta}$ (cubic, δ=0 ref. JCPDS 41-0253, δ=2 ref. JCPDS 41-0253). The nanopowders obtained by SPVD from these targets under 30-40 Torr air pressure were characterised by XRD. The analysis indicates again that two phases are present (see figure 12) : one was identified as $Zn_{1-x}Bi_xO$, yet seen in the targets, but the peaks corresponding to the other phase are related to $(Bi_{1-y}Zn_y)_2O_{3-z}$ close to β-Bi_2O_3 (tetragonal, ref. JCPDS 78-1793). The $Bi_{38}ZnO_{58+\delta}$ phase seen in the targets has vanished during the SPVD process.

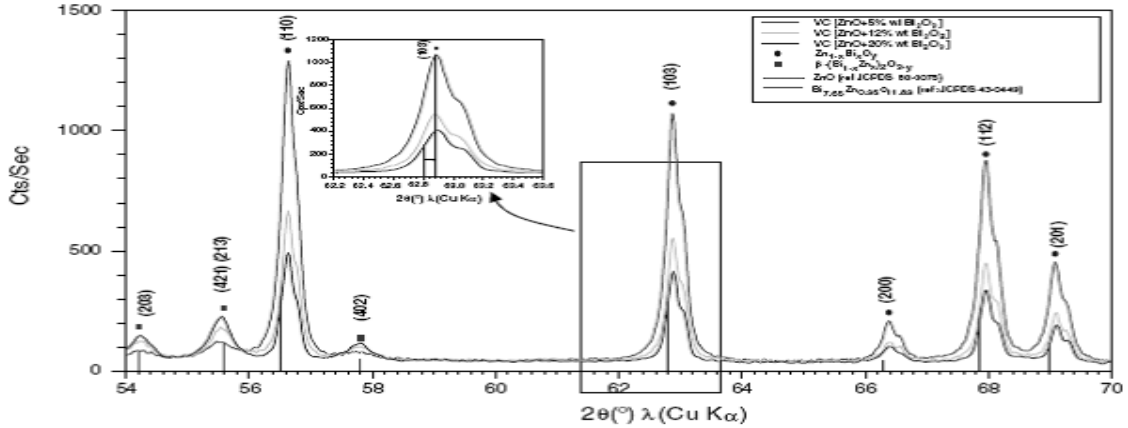

Figure 12 : XRD diagrams of nanopowders prepared by SPVD from targets made of mixtures of ZnO and Bi_2O_3

HRTEM studies have shown that for 5 wt% Bi_2O_3, the aspect is similar to pure ZnO nanopowders prepared in same conditions with a prevalence of nanowhiskers. Increasing the bismuth content, the morphology changes from whiskers to more compact shapes. Precipitates are visible, they are more and more numerous and less and less lengthened when the Bi content increases. The $(Bi_{1-y}Zn_y)_2O_{3-z}$ phase has a tetragonal character which explains the polygonal shapes of the observed precipitates (see figure 13).

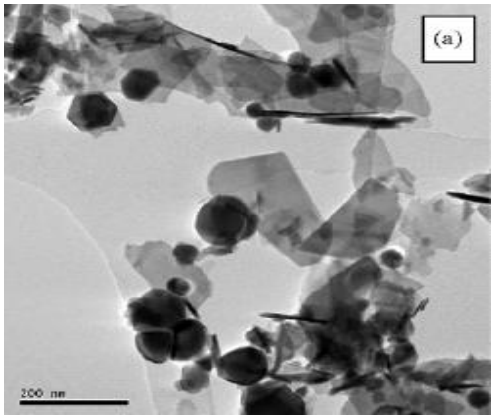

Figure 13 : TEM images from nanopowders prepared by SPVD using ZnO+20%wt Bi_2O_3 targets

Average nanophase sizes have been deduced from the diffraction peaks corresponding to $Zn_{1-x}Bi_xO$ in the XRD diagram of figure 12, the results are reported in figure 14. Increasing the Bi content of the targets, the $Zn_{1-x}Bi_xO$ nanophases are characterized by a decreasing "grain size", the smallest grain sizes (around 30nm) being obtained on nanopowders prepared by SPVD using ZnO+20%wt Bi_2O_3 targets. As the black (thick) precipitates in figure 12 have been identified as the Bi rich compound $(Bi_{1-y}Zn_y)_2O_{3-z}$, the $Zn_{1-x}Bi_xO$ solid solution correspond to the zinc rich transparent platelets. The decrease of their size could be due to their substructure or to twisted or/and tilted parts of the nanocrystals. Looking at the XRD peaks intensities, It is clear that the dominant phase in these nanopowders is $(Bi_{1-y}Zn_y)_2O_{3-z}$, which can be considered as Zn doped β-Bi_2O_3 and noted β-$(Bi_{1-y}Zn_y)_2O_{3-z}$.

From these nanopowders it is possible to prepare films or coatings or massive nanomaterials. The annealing treatment performed to sinter the nanopowders (820°C, 2 h in air) induces a new phase change : in the nanomaterial obtained two phases are present : $Zn_{1-y}Bi_yO$ and $(Bi_{1-x}Zn_x)_2O_{3-y}$ close to α-Bi_2O_3 (monoclinic, ref. JCPDS 71-2274) and accordingly noted α-$(Bi_{1-x}Zn_x)_2O_{3-y}$.

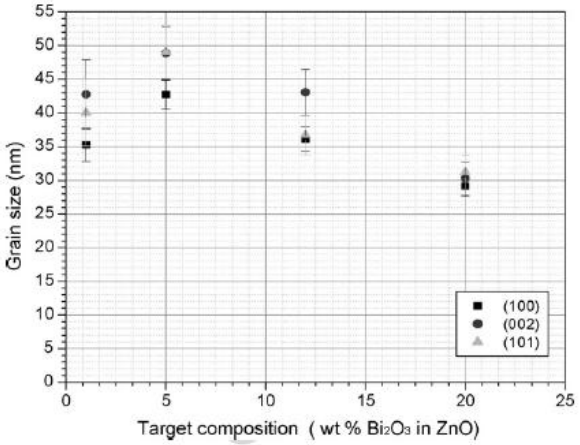

Figure 14 : $Zn_{1-x}Bi_xO$ nanophases grain size as a function of the Bi content of the SPVD target

The electrical conductivity of these nanocomposites has been measured by impedance spectroscopy, the results obtained at temperatures in between 110°C to 300°C are shown in the figure 15 and compared to the conductivity of α, β and δ-Bi_2O_3 [25], to the conductivity of the $Bi_{38}ZnO_{58+\delta}$ cubic phase (which has been synthesised separately) and to the conductivity of gadolinium doped ceria as a reference : the massive nanomaterials prepared from $(ZnO)_{95.2}(Bi_2O_3)_{4.8}$ nanopowders (obtained from ZnO+15wt%Bi_2O_3 mixtures) are the best ionics conductors in the considered temperature range, the $(ZnO)_{98.7}(Bi_2O_3)_{1.3}$ nanopowders (obtained from ZnO+5wt.%Bi_2O_3 mixtures) lead to nanomaterials less conductive. Bi rich phases $(Bi_{1-x}Zn_x)_2O_{3-\delta}$. are probably responsible for these results.

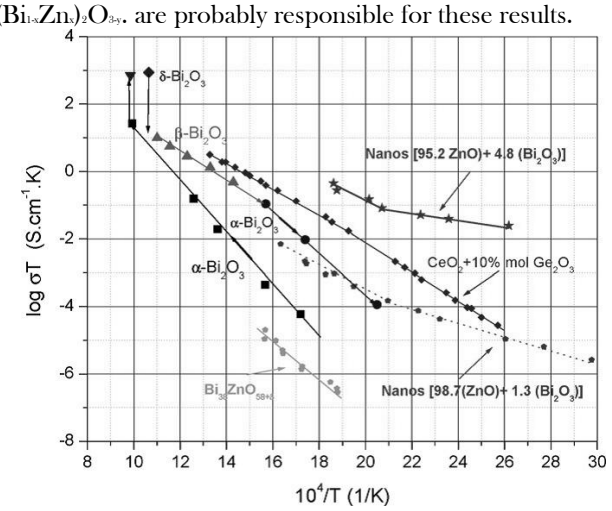

Figure 15 : ionic conductivity of several compounds compared in an Arrhenius diagram.

5-f Zn and ZnO_{1-x} nanophases[6, 12]

A preparation by SPVD of nanopowders from pure ZnO was carried out under argon flow at pressures from 2 Torr to 20 Torr (flows from 2 to 3 liters/min) in the solar reactor "heliotron". XRD diagram of the nanopowders show that the collected nanopowders were constituted by a mixture of metallic Zn (majority component) and strongly non-stoechiometric ZnO nanophases. This result shows that at high temperature under neutral gas flow, ZnO is dissociated according to the reaction :

$$ZnO \text{ ===> } Zn + \tfrac{1}{2}\, O_2(g) \qquad (4)$$

The produced Zinc is initially at the vapour state. Then, quickly, aggregates are formed. The oxygen produced is pulled out by the argon flow, that is not the case of the zinc aggregates. This distillation phenomenon leads to a zinc content in the nanopowders depending on the collecting position in the reactor.

The Zn nanoparticles produced are very reactive because of their small size. This property can be used to carry out chemical reactions at temperatures lower than those generally practised such as the decomposition of the water vapor :

$$Zn + H_2O(g) \text{ ===> } ZnO + H_2\,(g) \qquad (5)$$

Both reactions (4) and (5) constitute a cycle in which ZnO is conserved. The reaction (4) is endothermic and is a way to store solar energy in the form of heat which is restored partly by the exothermic reaction (5). At the same time hydrogen and oxygen are produced and can be separated and stored for a later use. In a recent work this SPVD process as been used to prepare mixtures of Zn and ZnO nanophases and their reactivity versus water vapour to produce hydrogen as been studied[26].

6. Characterisation and properties of TiO_2 based nanophases prepared by SPVD

6-a SPVD nanopowders of TiO_2 based nanopowders

TiO_2 based nanopowders were prepared using the Solar Physical Vapour Deposition (SPVD) process. Targets were prepared as compressed of 1cm in diameter and 5 to 8 mm height by sintering commercial powders of pure TiO_2 or of mixtures of TiO_2 with doping oxides (Fe, Co or Mn oxides). The vapor pressure around the target depends on the temperature and the atmosphere inside the balloon. At pressures larger than 10 Torr, a smoke is generally visible, it is more or less thick. The smokes are depositing by condensation on a cold finger (water cooled copper tube) located at a few centimeters above the target. The production rate of the nanopowders depends on the vapor pressure of the material. In the case of TiO_2 based targets, the material melts before vaporising, it starts to boil at temperatures in the range of 1500°C but droplets are produced which damage the balloon and it is necessary to limit the working temperature to avoid this phenomenon. In these conditions, the amounts of collected powders are of the order of 10mg/hour.

The nanopowders and targets were characterized by X-Ray Diffraction (XRD), Scanning Electron Microscopy (SEM) and Raman spectroscopy.

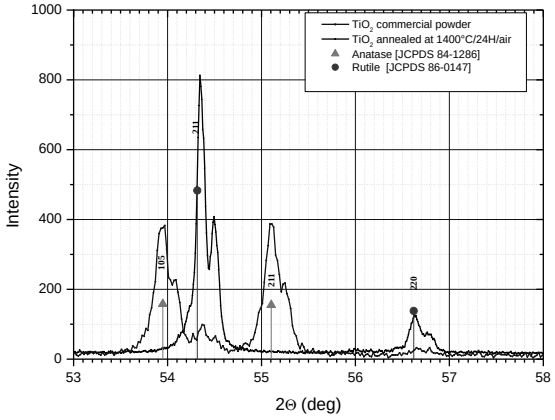

Figure 16 : XRD diagrams showing the transformation from anatase to rutile of the commercial TiO_2 by annealing at 1400°C in air during 24h.

6-b . Characterization of pure TiO_2 SPVD nanophases

6-b-1 XRD diagrams obtained on the targets

TiO_2 commercial powder used to prepare the targets was annealed at 1400°C under air, the X-rays diffraction diagrams obtained before and after annealing are shown in the figure 16. The peaks positions with their indexes referring to the Anatase and Rutile phases (JCPDS 84-

1286 and 86-0147) have been indicated. As already shown by other authors [27], these spectra indicates a dominating presence of the Rutile phase in the annealed powder while Anatase phase is much more abundant than the Rutile phase in the initial raw powder. It is noteworthy to remember that Anatase is generally considered as a metastable phase and Rutile as stable.

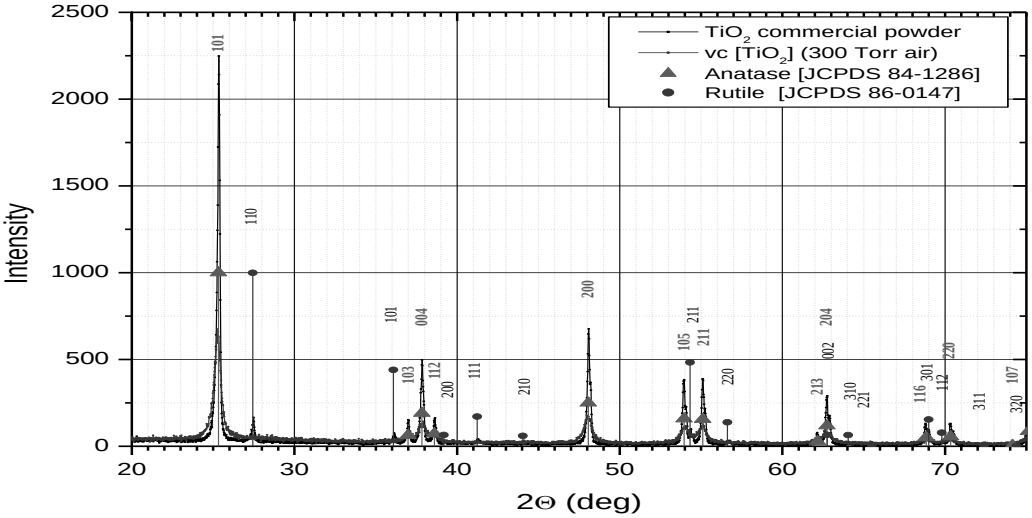

Figure 17 :. comparison between XRD diagrams obtained for a TiO_2 commercial powder and for the nanopowders obtained by SPVD under 300 Torr air pressure.

6-b-2 XRD diagrams obtained on pure TiO_2 nanopowders

Nanopowders were prepared by SPVD under air pressure in the heliotron solar reactor, starting from commercial TiO_2. At low air pressure, TiO_2 is melted before vaporization, and this caused sparkles damaging the reactor. Because of that, the air pressure was maintained up to 90 Torr. The figure 17 shows a diagram obtained on SPVD nanopowders prepared at 300Torr air pressure.

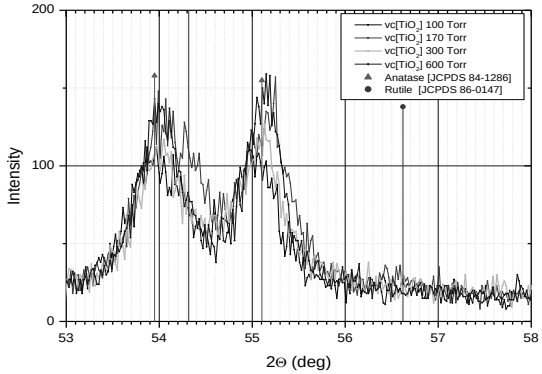

Figure 18-a : Influence of the air pressure inside the solar reactor on the appearance of the anatase (105 and 211 peaks) or rutile phase (211 and 220 peaks) in SPVD nanopowders.

The figure 18 shows a detail of the XRD diagram obtained on the collected nanopowders as a function of the air pressure flowing in the reactor. The variation of the gas pressure in the reactor has an impact not only on the size of the nanophases but also on their crystallographic structure.

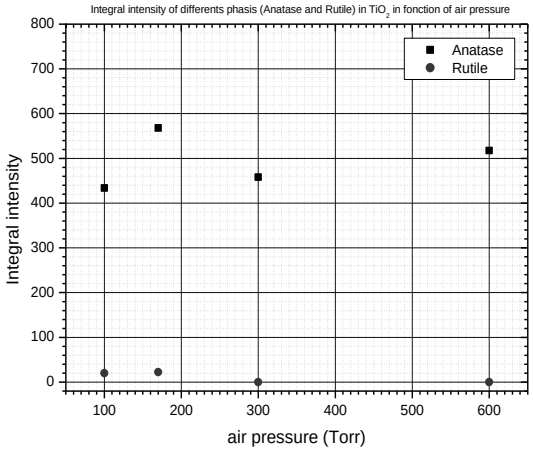

Figure 18-b : Influence of the air pressure inside the solar reactor on the integrated intensities of XRD peaks 101 and 110, corresponding respectively to anatase or rutile.

The figure 18-b shows the evolution of the 110 and 101 peak intensity corresponding respectively to the Rutile phase and to the Anatase phase in function of the air pressure in the reactor. It can be observed on the XRD diagram obtained from nanopowders prepared under 100 and 170 Torr air pressure that the Anatase phase is the majority one and that the intensity of the Rutile peaks decreases gradually. At 300 Torr and at 600 Torr air pressure the Rutile peaks have disappeared.

6-b-3- Raman spectroscopy of pure TiO_2 nanopowders

Nanopowders prepared by SPVD have been studied by Raman scattering and the results compared to those obtained on the commercial powder used to prepare targets. The figure 19 shows that the starting raw material is an heterogeneous mixture of Anatase and Rutile in which Anatase is dominant.

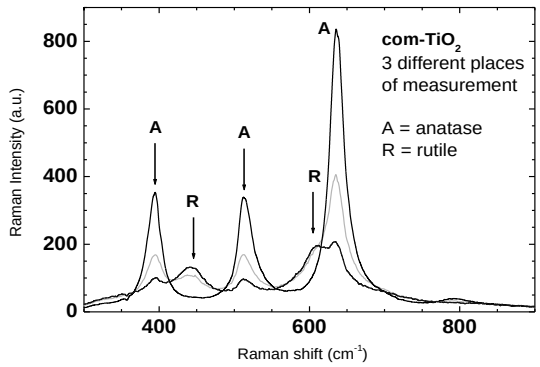

Figure 19 : Raman spectroscopy performed on three samples of the commercial TiO_2 powder

The obtained SPVD nanopowders (see figure 20) are in the Anatase phase when the air pressure in the reactor is higher than 100 Torr and in the Rutile phase below 150 Torr. This is in good agreement with the XRD analysis results (see figures 17, 18-a and b).

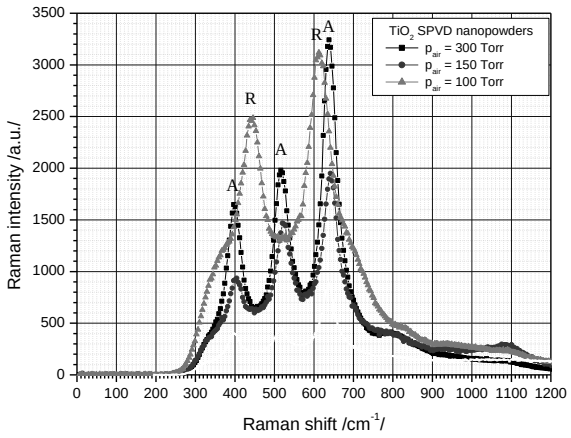

Figure 20 : Raman spectroscopy performed on TiO_2 SPVD nanopowders.

6-b-4 Average grain sizes of pure TiO_2 nanopowders

The procedure presented in §4-b has been used to calculate the grain sizes of the differents phases appearing in the XRD diagram of the nanopowders. The dependence of the average "grain size" of the appearing nanophases as a function of the air pressure during the SPVD process is reported in the figure 21.

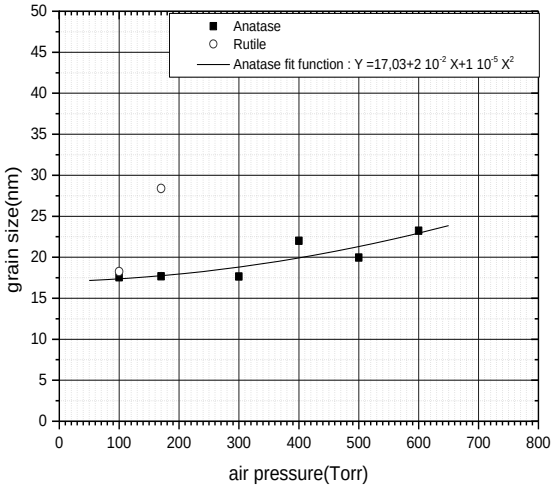

Figure 21 : Average size of the SPVD anatase and rutile nanophases versus air pressure inside the solar reactor.

From figure 21 it appears that these nanopowders are characterized by very small grain sizes. The average grain size of anatase (which is the majority phase) remains practically constant (<18 nm) until 300Torr ; it increases at higher pressure (23nm at 600Torr). The Rutile phase increases in size from 18nm at 100Torr to more than 24nm at 170Torr and vanishes. A fit to the experimental values by a second order polynomial leads to the expression :

$$y = 1\,10^{-5}\,p^2 + 2\,10^{-2}\,p + 17.03 \qquad (6)$$

where the air pressure p is given in Torr and the average grain size y is in nanometers.

Calculations of grain sizes have been carried out from BET measurements using the relation (7).

$$d_m = \frac{6}{S\rho} \times 1000 \qquad (7)$$

Where d_m is in nm when S, the specific BET surface area, is in m^2/g and ρ the picnometric density of the nanopowders is in g/cm^3 (to have a circular form the powder grains are assumed). The results are gathered in table 1.

As BET is sensitive to the surface of the particles and the fact that the particles have similar shapes (see figures 22-a and 22-b), the agreement between the BET and the SEM images is not surprising. Nevertheless there is a large discrepancy between BET and XRD, specially for the nanopowders. The fact that BET measurements lead to a larger grain size than XRD indicates that the grains are nanostructured. SEM images of these nanopowders (see figure 22-b) suggest that the grains of the nanopowders are in fact aggregates (the surface roughness of the grains of the nanopowders is larger than for the commercial powder, many small grains are connected to the large ones).

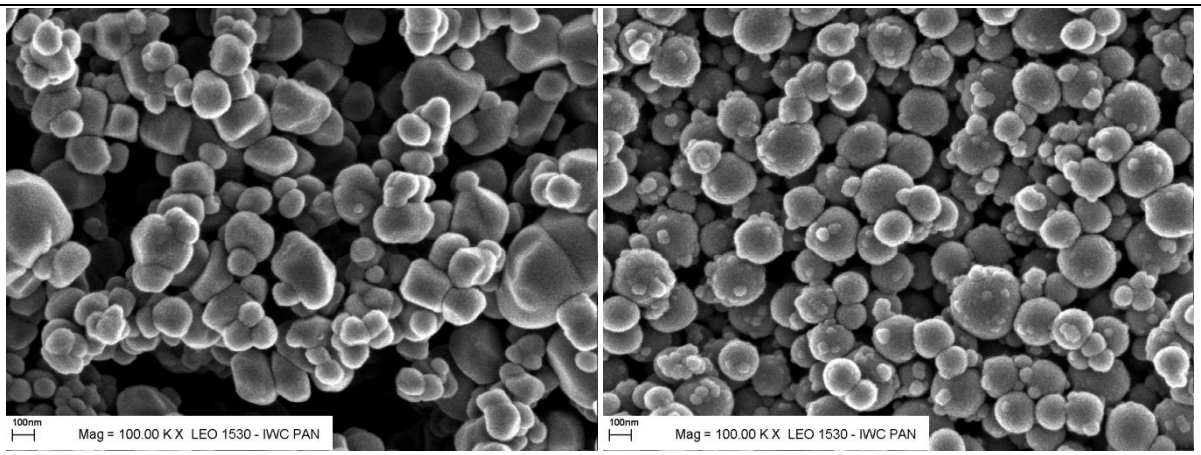

Figures 22-a and 22-b : SEM images of pure TiO_2 commercial powder (a) and SPVD nanopowder (b).

Table1

TiO_2	BET [m^2/g]	Density [g/cm^3]	Average grain size from BET (nm)	Average Grain size from XRD (nm)
Commercial Raw	8.871	3.885	174	57
SPVD nanopowder (300 Torr air)	9.112	3.867	170	18

7. Characterization of Fe, Co or Mn doped TiO_2 SPVD nanopowders

7-a XRD analysis of the Fe, Co or Mn doped TiO_2 nanopowders

The figure 23 shows an example of XRD diagram obtained on a Fe-doped TiO_2 as-prepared target ($Ti_{0.98}Fe_{0.02}O_2$) : as the anatase phase does not appear in XRD diagram, one can consider the majority phase is rutile.

Nanopowders were prepared by SPVD using Fe, Co or Mn doped TiO_2 targets ($Ti_{1-x}M_xO_2$ x is the atomic fraction of M taking the values : 0.01, 0.02, 0.05). The figure 24 shows the XRD diagram obtained on $Ti_{0.95}M_{0.05}O_2$ (M=Co,Fe or Mn) nanopowders prepared under flowing air, the pressure inside the solar reactor being maintained at 10 Torr and the figure 25 corresponds to $Ti_{0.99}M_{0.01}O_2$ (M= Fe, Co or Mn) nanopowders prepared under 90 Torr.

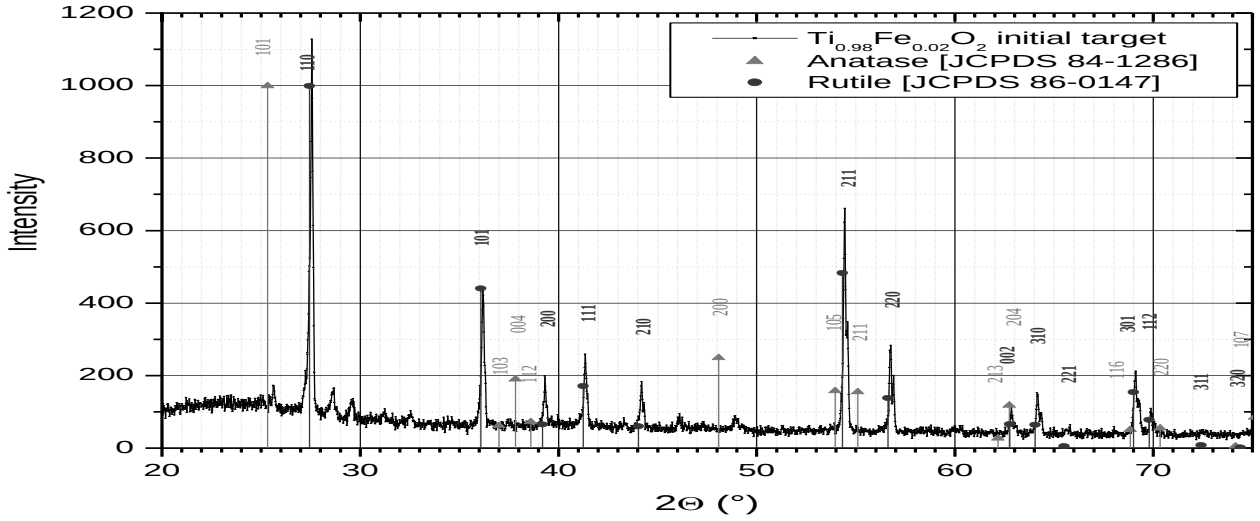

Figure 23 : XRD diagram of a $Ti_{0.98}Fe_{0.02}O_2$target. The majority phase is rutile.

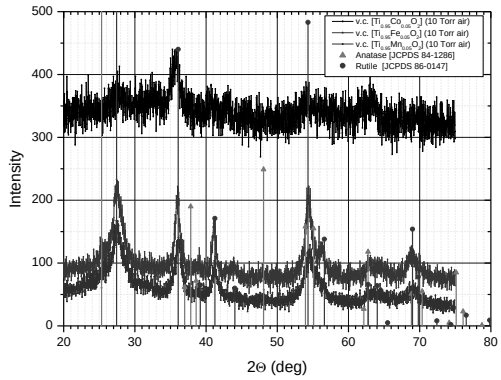

Figure 24 : XRD diagram obtained on $Ti_{0.95}M_{0.05}O_2$ (M=Co,Fe or Mn) SPVD nanopowders prepared under 10Torr air

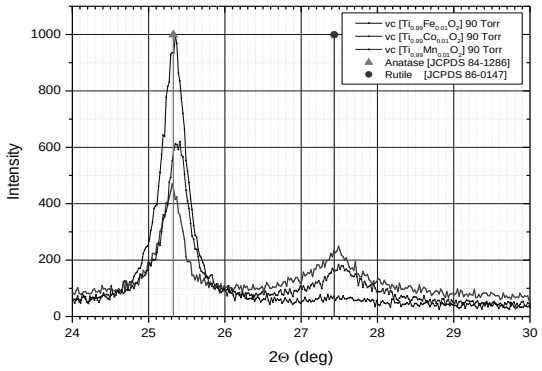

Figure 25 : $Ti_{0.99}M_{0.01}O_2$ (M= Fe, Co or Mn) nanopowders prepared under 90 Torr

The $Ti_{0.95}M_{0.05}O_2$ nanopowders produced under 10 Torr air are essentially in the Rutile phase, the contribution of Anatase is below 5%. For the $Ti_{0.99}M_{0.01}O_2$ nanopowders prepared under 90 Torr the majority phase is Anatase but the Rutile phase appears significantly for the Co or Mn doped samples. In the case of $Ti_{0.99}Fe_{0.01}O_2$, experiments performed at higher air pressure (100Torr and 300Torr) led to similar results as the experiments performed at 90 Torr for $Ti_{0.99}Co_{0.01}O_2$ and for $Ti_{0.99}Mn_{0.01}O_2$. Remembering that the metastable rutile phase has been clearly observed only around 170 Torr for pure TiO_2 during the SPVD process, the observations show that doping at low levels tends to stabilize the rutile phase.

7-b Dependence on air pressure of the nanostructure of the Fe doped TiO_2 nanopowders

The evolution of the diagrams obtained on Fe-doped TiO_2 nanopowders ($Ti_{0.99}Fe_{0.01}O_2$) for two different values of the air pressure inside the reactor is shown in the figure 26.

It can be observed that the ratio of the intensities of two peaks, one belonging to the Anatase phase and the other to the Rutile phase, increases with the pressure.
The shape of the peaks already confirms the observations done under this vaporization air pressure. The peaks intensity of the Anatase phase is even more intense in the case of 300 Torr compared to 100 Torr air. The grain size calculations led to 36 nm for the Anatase phase and 12 nm for the Rutile phase (see table 2).

Table 2

$Ti_{0.99}Fe_{0.01}O$ sample	Grain size (nm)	
Air pressure (Torr)	Anatase(101)	Rutile(110)
initial target	-	52.2
100Torr vc(initial target)	31.2	11.1
300Torr vc(initial target)	35.95	12.5

Table 3

$Ti_{0.98}Fe_{0.02}O$ sample	Grain size (nm)	
Air pressure (Torr)	Anatase(101)	Rutile(110)
initial target	-	69
100 Torr vc(initial target)	10.6	5.0
200 Torr vc(initial target)	40.0	12.4
300 Torr vc(initial target)	43.9	6.0

Similar measurements have been carried out on $Ti_{0.98}Fe_{0.02}O_2$ (see table 3). HRTEM observations show that the particles size is in between 10nm and 30nm (see figure 27 a) with a large mosaicity (see figure 27 b). The small "grain sizes" determined by XRD on the nanopowders (≅ 5 nm for this $Ti_{0.95}Fe_{0.05}O_2$ nanopowders) are hence linked in fact to the substructure size. EELS (Energy Electron Loss Spectroscopy) measurements indicate that the distribution of Fe in the Rutile phase is homogeneous[28].

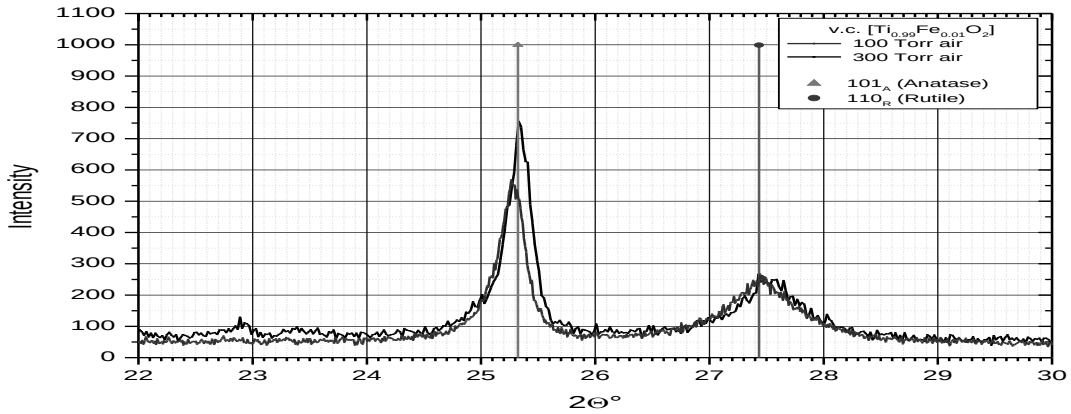

Figure 26 : XRD of SPVD nanopowders ($Ti_{0.99}Fe_{0.01}O_2$) prepared at two different air pressures : 100Torr and 300Torr (detail of the whole diagram).

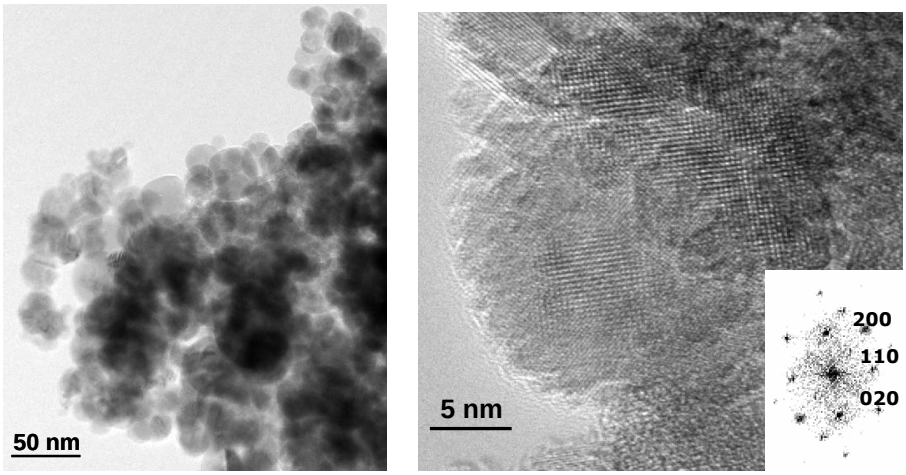

Figures 27-a and 27-b : HREM of Fe doped TiO_2 nanopowders prepared by SPVD.
Magnetic measurement and Mössbauer Spectroscopy of Fe doped TiO_2 nanopowders ($Ti_{0.95}Fe_{0.05}O_2$) performed at T=5K, showed that these nanophases are not ferromagnetic but in a paramagnetic state [28].

8. Discussion about the TiO_2 phase stability

Well annealed pure TiO_2 commercial powders are in the Rutile phase. It has been shown in this work that pure TiO_2 nanopowders prepared by SPVD are in the Anatase phase. For air pressure up to 100Torr, the Rutile phase does not appear. At the lowest pressures studied (100 and 170 Torr air), the Rutile phase appears as a minority phase beside the Anatase. Raman spectra is in agreement with the XRD analysis.

These result can be interpreted by capillarity effects : due to their small size and to the surface tension, the pure TiO_2 nanoparticles are stabilised in the Anatase phase. In addition, a thermokinetic effect can also be considered. At high pressures indeed, the air flow in the reactor is smaller than at low pressures and the cooling rate of the smokes produced during the SPVD process, is slower. At low pressures the phase transformation from Rutile to Anatase is not fully achieved. This is well supported by the observed increase of the average grain size while the pressure increases.

In doped TiO_2 targets made with annealed mixtures of powders, the Rutile phase is the majority phase. After vaporisation-condensation under low pressure and with a high dope content of the target, the majority phase is the Rutile but at low dope content and with high pressure during the SPVD process, leads to the decrease of the Rutile amount compared to the Anatase one.

The addition of dopes leads to stabilise the Rutile phase but the increase of the pressure has again the same effect as for pure TiO_2 : the Rutile phase amount is less and less important while the pressure increases at constant composition of the target. Using the same arguments as for pure TiO_2 it seems that the surface tension of doped particles decreases when a dope is present, the effect of the air pressure being similar to what has been explained for pure TiO_2. An investigation of surface segregation phenomena in this system could enlighten on this problem.

9. Preparation, characterisation and properties of magnetic composite nanophases

In the previous examples presented earlier nanopowders were obtained from targets prepared in conditions where the nanophases, component of the nanopowders, were expected to be simple and unique. In fact it has been seen,

it was not the case, the stability of the nanophases appearing being not ascertained in all cases including simple cases such as the classical unstable γ–Fe_2O_3 [29] or the case of TiO_2, where two phases, one being unstable, appear in proportions varying with the SPVD conditions. In the more complex case of targets made of ZnO+Bi_2O_3, two kinds of nanophases or more appear but that's less surprising.
To offer an alternative to chemical processes biologically not fully satisfying, a program of preparation by SPVD of nanoparticles used in medicine as markers for magnetic resonance imaging and heating mediators and preserving their biological environment was proposed. The idea was to prepare composite nanophases made by a magnetic core surrounded by a bio-compatible shell. The challenge being to do that by SPVD.
Good results have been obtained with Fe nanoparticles coated with MgO [13].

Targets were obtained by mixing and pressing pure Fe and MgO powders with an excess of Mg in such a way to keep reducing conditions. The SPVD process was performed in an argon flow.
XRD diagram performed on the nanopowders is shown in the figure 28. The MgO peaks and Fe peaks are clearly distinct. HREM images show the core-shell nanostructure of the composite nanophases obtained (see figure 29). Figure 30 shows their magnetic behaviour[13].

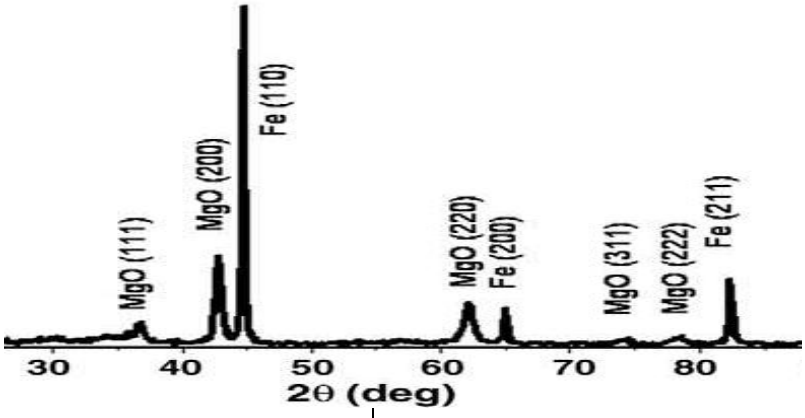

Figure 28 : XRD diagram of SPVD MgO coated Fe composite nanophases

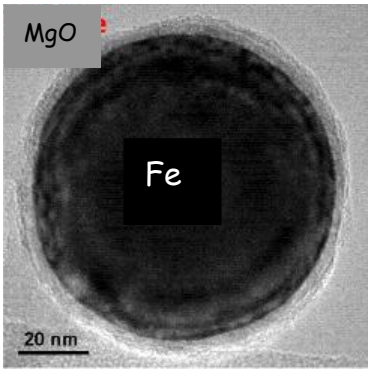

Figure 29 : MgO coated Fe nanophases prepared by SPVD. The magnetic properties of such composite nanophases have been determined. They behave as ferromagnetic .

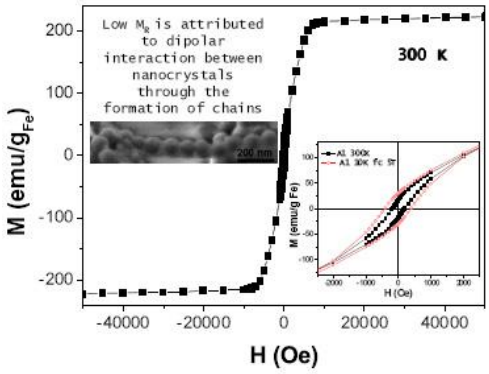

Figure 30 Magnetic behaviour of MgO coated Fe nanophases.
The low field region (inset) show a weak hysteresis effect.

Biological tests have demonstrated the stability of such nanoparticles. Their biocompatibility and their affinity for particular cells of the liver, spleen or kidneys lead to use them for magnetic imaging and targeted treatment of human diseases by hypothermia.

10.Conclusion

Several types of nanopowders were prepared in order to know the influence of the grain size on the known properties of materials. If new properties appear, specially at small grain size (nanomaterials), they open new fields of research. In many cases, it is on massive nanomaterials or in layers, that appear the new properties and the preparation of these nanomaterials is an important stage to cross. Among the compounds prepared by SPVD, we were focused in this study on ZnO based nanophases. $Zn_{1-x}Al_xO$, when it is prepared by SPVD, appears to be a remarkable blue emitter by luminescence and can be used to build luminescent screens or sensors. $Zn_{1-x}Co_xO$ is generally paramagnetic but can exhibit a ferromagnetic behaviour in

the form of nanopowders and could be used in optoelectronics.

The bi-phased compounds $Zn_{1-x}Bi_xO$-$(Bi_{1-y}Zn_y)_2O_{3-z}$, have very interesting electrical properties and they could be used as electrolytes in SOFC working at temperatures as low as 400°C. Production of metallic Zn nanophases could be a powerful solution to the solar energy storage and/or hydrogen production. Composite nanophases, such as the MgO coated Fe nanoparticles core-shell nanostructured, open new possibilities for medicine because of their biocompatibility and magnetic properties.

The few examples presented here highlight the interest of SPVD methods to work on nanopowders with remarkable properties it still remains to discover the best way of implementing them in the applications.

Acknowledgements

Many results presented here wer obtained in the frame of collaborative works supported by the European programs SOLFACE and SFERA. The managers of this helpful sponsoring are greatly acknowledged.

References

[1] C.J.A. Monty, The Arabian Journal for Science and Engineering, 35, 1C, (2010)93-116.

[2] C.J.A. Monty, High Temperatures and Chemical Process. 3, (1994)467-480.

[3] G.C. Hadjipanayis, R.W. Siegle,. *Nanophase Materials : Synthesis – Properties – Applications.* Series E : Applied Sciences, vol. 260, Kluwer Academic Publishers, Dordrecht, (1994)

[4] A. Rouanet, G. Pichelin, C. Roucau, E. Snoeck, C. Monty, Nanophase Materials; Kluwer Academic Publishers: Dordrecht, the Netherlands, (1994)85-88.

[5] A. Rouanet, H. Solmon, G. Pichelin, C. Roucau, F. Sibieude, C. Monty, Nanostructured Materials. 6(1-4), (1995)283-286.

[6] C. Monty, Ecole d'Eté CNRS, St. Pierre d'Oleron. (2005)231-259.

[7] J. Friedel, Phase transitions, 24-26 (1990) 215-227.

[8] C.J.A. Monty, A. Rouanet, F. Sibieude, Materials Science Forum. (1998)269-272, 297-302.

[9] N. Boulares, K. Guergouri, R. Zouaghi, N. Tabet, A. Lusson, F. Sibieude, and C. Monty, Physica Status Solidi (a), **201**, 10, (2004)2319-2328.

[10] C. Monty, Ionics, 8(5-6), (2002)461-469.

[11] T. Ait Ahcene, C. Monty, J. Kouam, A. Thorel, G. Petot-Ervas, A. Djemel, J. European Ceramic Society. 27, (2007)3413-3424.

[12] J. Kouam, T. Ait Ahcene, A.G. Plaiasu, M. Abrudeanu, A. Motoc, E. Beche, C. Monty, Solar Energy, 82, (2008)226-238.

[13] C. Martinez-Boubeta, Ll Balcells, R. Cristòfol, C. Sanfeliu, E. Rodriguez, E. Weissleder, S. Lope-Piedrafita, K. Simeonidis, M. Angelakeris, F. Sandiumenge, A. Calleja, L. Casas, C. Monty, and B. Martínez., Nanomedicine : Nanotechnology, Biology, and Medicine, NANO-00307 (2009).

[14] F. Teixera, R. Berjoan, G. Peraudeau, D. Perarnau, Solar Energy. 78(6), (2005)763-771.

[15] G. Flamant, , D. Luxembourg, , J-F. Robert, , D. Laplaze, , *solar reactor*. Solar Energy. 77, (2004)73-80.

[16] L. Bragg, *The crystalline state*. G. Bell Londres, **1**, 1949.

[17] J.I. Langford, D. Louër, E.J. Sonneveld, J.W. Visser, Powder Diffraction. 1(3), (1986)211-221.

[18] C. Boudias, D. Monceau, 1989-2005, http://pros.orange.fr/carine.crystallography/

[19] R.R. Piticescu, B. Malic, M. Kosec, A. Motoc, C. Monty, I. Soare, T. Kosmac, A. Daskobler, J. European Ceram. Soc. 24(6), (2004)1941-1944.

[20] R.R. Piticescu, R.M. Piticescu, C. Monty, J. European Ceram. Soc. 26, (2006)2979-2983.

[21] J. Grabis, Dz.Jankovica, M. Berzins, L. Chera, I. Zalite, J. European Ceram. Soc. 24(2), (2004)179-184.

[22] L. Grigorjeva, D. Millers, K. Smits, C. Monty, J. Kouam, , L. El Mir, Solid State Phenomena 128, (2007)135-140.

[23] T. Strachowski, E. Grzanka, W. Lojkowski, A. Presz, M. Godlewski, S. Yatsunenko, H. Matysiak, R.R. Piticescu, C.J. Monty, Journal of Applied Physics 102, (2007)073513.

[24]B. Martínez, F. Sandiumenge, L. Balcells, J. Arbiol, F. Sibieude, C. Monty, Appl. Phys. Lett. 86, (2005)103-113.

[24] B. Martínez, F. Sandiumenge, L. Balcells, J. Fontcuberta, F. Sibieude, C. Monty, J. Appl. Phys. 97, (2005)10D311.

[24] B. Martínez, F. Sandiumenge, L. Balcells, L. Arbiol, F. Sibieude, C. Monty, J. Phys. Rev. B. 72, (2005)165202 .

[25] O. Monnereau, L. Tortet, P. Llewellyn, F. Rouquerol, G. Vacquier, Solid State Ionics. 157, (2003)163-169.

[26] M. Chambon, S. Abanades, G. Flamant, International Journal of Hydrogen Energy 34, (2009)5326-5336.

[27] C.N. Rao, and K.J. Rao, *Phase transitions in solids*. chap 2, McGraw-Hill, New York (1978)

[28] Ll. Balcells, C. Frontera, F. Sandiumenge, A. Roig, B. Martinez, J. Kouam, and C. Monty, Appl. Phys. Lett., **89**, (2006)122501-3.

[29] B. Martinez, X. Obradors, L. Balcells, A. Rouanet, C. Monty, Phys. Rev. Lett. 80, (1998)181-184.